Acta Cryst. (1991). A47, 707-715

A Robust Solution for RHEED

BY Y. MA* AND L. D. MARKS

Department of Materials Science and Engineering, Northwestern University, Evanston, IL 60208, USA

(*Received 7 February* 1991; *accepted 14 May* 1991)

Abstract

A new method of solving the reflection diffraction problem using a stabilized edge in a multislice-type calculation is described. Results that compare it with Bloch-wave calculations show that it is a very robust solution and for one surface raises an important issue concerning the boundary match in the Bloch-wave approach. It is shown that the standard boundary match used is often invalid for reflection problems and may also be questionable for transmission problems although here the effects will be smaller. The correct boundary match on a surface which need not be flat is described.

I. Introduction

An area of some recent interest is the improved methods of understanding reflection high-energy electron diffraction patterns and its partner reflection electron microscopy. One of the main issues which is currently under intense scrutiny is the method of extending from simple limited-beam dynamical calculations of simple surfaces to more general many-beam dynamical calculations of general surfaces. At present three different methods are under development. The first is a transfer of LEED (low-energy electron diffraction) calculation methods to the RHEED (reflection high-energy electron diffraction) case pioneered by Maksym & Beeby (1981) which appears to be a powerful method of generating rocking curves from simple surfaces with 2D periodicity. The second is the Bloch-wave approach which dates back to the 1930's (Shinohara, 1932) where the bulk Bloch-wave solutions are matched at surface to vacuum plane waves. The third method is to exploit the fast numerical multislice method to simulate surface reflection as introduced by Peng & Cowley (1986).

All these methods have some problems, and we will briefly discuss some of them for the last two methods since this will be relevant to later sections of this paper. Two critical problems with the Bloch-wave method have been the surface matching and the identification of the excited Bloch waves in a semi-infinite crystal. The standard Bloch-wave-matrix method (Metherell, 1975) leads to $2N$ eigensolutions and $n \times N + 2N$ unknowns (n denotes the number of boundaries and N the number of active Fourier coefficients of the bulk potential) constrained by $n \times 2N$ boundary conditions. $n \times N$ represents the number of coefficients of the plane waves outside the crystal while $2N$ is the number of excitation coefficients of all possibly active Bloch waves inside the crystal. For the transmission case, both the back-reflected Bloch waves and the bottom boundary can be omitted. Then we have $1 \times N + N$ unknowns constrained by $1 \times 2N$ boundary conditions. However, for reflection cases, the N back-reflected Bloch waves which are not excited inside the crystal can no longer be easily identified. Colella (1972) and Moon (1972) used an approach for the case where absorption is included by modelling the system as a crystal slab with a pair of surfaces semi-infinitely separated. Owing to the absorptive attenuation, there are actually only N Bloch waves excited in the crystal slab although $2N$ solved Bloch waves are all taken into account. In that case, there are $2 \times N + 2N$ unknowns constrained by $2 \times 2N$ boundary conditions. To identify N Bloch waves excited in a semi-infinite crystal and avoid introducing the bottom boundary, the current flow argument was introduced by the authors (Marks & Ma, 1988; Ma & Marks, 1989, 1991), which is equivalent to Collela's argument in the presence of absorption. However, all these arguments are based upon a planar boundary match. More recently, it has been pointed out by Kambe (1988) that one can simplify the bulk matrix for a low-index surface, although the simplification itself does not overcome the issue of boundary match and it just reduces the size of the numerical problems. Although how to match at the boundary is better understood now, a critical issue is still there: the effects of discontinuities between the terminated bulk-crystal potential and the zero vacuum potential and the associated neglect of any surface potential. The critical numerical tests for simple Au(001) surfaces in the [010] zone were carried out by the authors (Ma & Marks, 1990*a*, *b*, 1991). The tests showed no major problem. However, we will return to this point later to demonstrate that on more complicated surfaces this is a major issue.

* Current address: Department of Physics, University of Oslo, PO Box 1048, Blindern, 0316 Oslo 3, Norway.

0108-7673/91/060707-09$03.00 © 1991 International Union of Crystallography

The multislice approach is powerful due to the proliferation of multislice programs, but results suffer from edge effects. Owing to the limitation of simulation size of an incident beam in a numerical unit cell, a stationary solution for a virtually infinite incident wave becomes hardly obtainable. Although one can certainly obtain substantial physical information from a conventional multislice approach, for instance, a real-space picture of the scattering process, a troubling issue is to what extent this represents a true stationary solution in a semi-infinite crystal and what artifacts are introduced by the edges of the top-hat incident wave.

The primary focus of this paper is to describe a modification of the multislice method which has been discussed in part in a previous short report (Ma, 1990*b*). The method appears to stabilize reflection solutions against edge effects making rapid calculations of general surfaces quite straightforward; we will compare the results of this approach with those of the Bloch-wave and simple multislice methods for three different surfaces, namely Au(100) in the [010] zone; 2×1 reconstructed Au(001) in the same zone and finally for Au(110) in the [1$\bar{1}$0] zone. Interestingly, for the Au(110) surface the Bloch-wave methods fail quite badly which has been reported in a previous short report (Ma, 1990*a*). We will show in the discussion that it is due to a failure of the conventional plane-surface matching between the bulk and vaccum. The source of this failure is discussed.

II. Theoretical basis and numerical methods

The key theoretical fact that we will exploit has been described previously (Ma & Marks, 1989) and is quite straightforward; we will briefly recap it here. With a standard Green function, we can write the Schrödinger equation in its integral form:

$$\psi(\mathbf{r}) = \exp(i2\pi\mathbf{k}\cdot\mathbf{r}) - (2m/4\pi\hbar^2)\int G(\mathbf{r}-\mathbf{r}')V(\mathbf{r}')\psi(\mathbf{r}')d\mathbf{r}'. \quad (1)$$

Then this can be expanded as an iterative sequence (assuming that the wave field does not diverge) as

$$\psi_n(\mathbf{r}) = \exp(i2\pi\mathbf{k}\cdot\mathbf{r}) - (2m/4\pi\hbar^2)\int G(\mathbf{r}-\mathbf{r}')V(\mathbf{r}')\psi_{n-1}(\mathbf{r}')d\mathbf{r}' \quad (2)$$

where $\psi_n(\mathbf{r})$ is the nth-order approximation to $\psi(\mathbf{r})$. We next exploit the fact that due to the translational symmetry of a RHEED problem (Ma & Marks, 1991), we have

$$\psi(\mathbf{r}) = \psi(\mathbf{q}, y) = \psi'(\mathbf{q})\exp(i\alpha y') \quad (3)$$

where $\mathbf{q}$ is a real-space vector in the xz plane, the y axis is along the incident beam and y' is a multiple of the surface translational symmetry along y. Combining (2) and (3) and considering Ishizuka & Uyeda's (1977) derivation, we can rewrite the series expansion (2) in the form of the multislice formulation of Cowley & Moodie (1957, 1959):

$$\psi'(\mathbf{q})\exp[i(n)\alpha\Delta y] = \{\psi'(\mathbf{q})\exp[i(n-1)\alpha\Delta y] \times P_g(\mathbf{q}, \Delta y)\}^* P_r(\mathbf{q}, \Delta y) \quad (4)$$

where Δy is the slice thickness of each iteration taken here as the translational repeat along y. (We note that the right-hand side can be expanded as a series of multislice steps if Δy is fairly large.) Equation (4) shows two aspects of the multislice iteration in the Bragg case: on one hand, for $\psi'(\mathbf{q})$, each iteration is equivalent to a Picard iteration cycle; on the other hand, each iteration makes a constant increment in phase $\exp(i\alpha\Delta y)$ to the wave function. The input wave is the first trial wave function and the nth multislice output is the nth approximation to the correct result. The difference between the stationary wave fields of any two slices is only a constant phase term: $\exp(im\alpha\Delta y)$.

The above analysis indicates that the multislice method, albeit used in a different context, generally should be able to solve RHEED problems. However, the problem of the edges remains. It results from artificially cutting off the infinite incident plane wave at the end of each slice because of size limitations in the numerical unit cell. The trick of solving the problem is to exploit (3) and (4) again, recognizing that the inward moving edge in the numerical unit cell will not have the correct behavior, but the standing-wave component will. Therefore, what we can do is to patch the deteriorated edge region of the unit cell at $y+n\Delta y$ by replacing it with the corresponding region at y which has not deteriorated, as long as it is multiplied by a constant phase $\exp(i\alpha n\Delta y)$. If we do this, we are also physically adding an additional part of the incident wave to the numerical solutions at a depth $y+n\Delta y$. The physical picture of the numerical simulation is therefore (as n tends to infinity) one of an infinite incident plane wave; an outside (vacuum) edge which never reaches the surface if the patching is done correctly; an inner (near the surface) edge which will vanish at large depths; the vacuum Bragg reflected waves; and the crystal Bloch waves which will exactly match the true wave field over a limited region for a semi-infinite system. Physically, the patched region plays the role of an infinite plane-wave source in a finite numerical unit cell. The trick here is that the wave front of the Bragg reflected waves always moves away from the crystal, while only the wave front of the incident plane wave moves towards the crystal. This means that any other reflected-wave components in the not-deteriorated edge region at y have no effect on the stationary solution at $y+n\Delta y$ in the region close to the surface

which we are searching for. Therefore, as long as we have the incident plane-wave component not deteriorated in the region at y and preserve the phase continuity of the incident plane wave for each patching, the iteration can be carried out to infinity. In other words, the edge-patching method will also work for a simple plane wave as a trial function. This procedure is illustrated in Fig. 1.

To implement this, we have used a standard rectangular unit cell in the multislice calculations, with the phase term α numerically calculated (an analytical method would presumably do as well). The maximum iteration number n at which the patching should be done is calculated according to the rate of the edge deterioration which primarily depends upon two parameters: incident angle (θ_0) and slice thickness (Δy). The patching has been implemented on the left outer part of the unit cell ($0 < z < 0{\cdot}25$, where z is normal to the surface, *i.e.* from A to B in Fig. 1) with the crystal located in the region $0{\cdot}75 < z < 1{\cdot}0$ (from C to D in Fig. 1). We have tested the approach with both a simple top-hat plane wave as the first trial solution and with the results of a Bloch-wave calculation as the input wave for the Au(001) surface in the [010] zone: the results stabilize in both cases but the better the initial guess is, clearly the faster the convergence of the method will be.

The key test of the method is whether a stationary solution is reached and in the subsequent section examples will be shown.

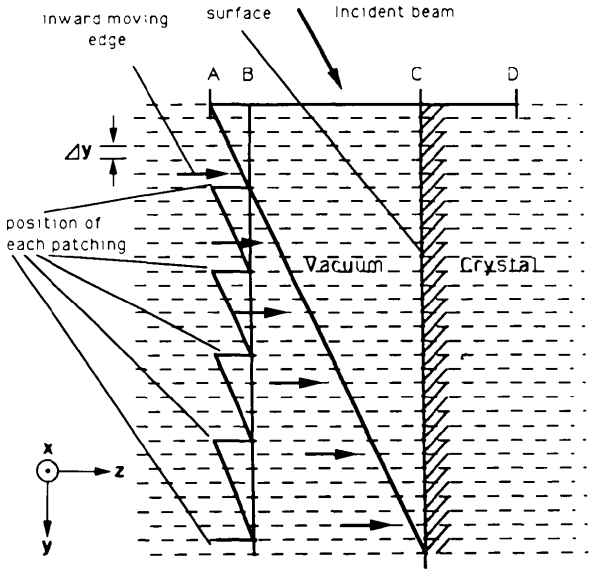

Fig. 1. Schematic diagram of the beam geometry of RHEED and the numerical treatment of the edge-patching method. The numerical unit cell is located from A to D. The arrows indicate the inward-moving edge. The surface is at C. The range from C to D contains the crystal. The patched-edge region is located from A to B and the stationary solution is obtained in the region from B to D.

III. Results

As an example of the method, Fig. 2 shows a comparison of the results for the patching with an incident plane wave, patching with an input Bloch-wave solution and a simple top-hat multislice with an input Bloch-wave solution for the Au(001) surface in the [010] zone. [For details of the latter two methods see Ma & Marks (1989, 1990*a*).] The difference between the iteration numbers of any two nearest slices in Figs 2 (i)-(iii) is 100 and the slice thickness of each iteration $\Delta y = 1{\cdot}012$Å. Comparing the three:

(*a*) The solution of the patching method with a top-hat incident wave [Fig. 2(i)] stabilizes after about 600 Å.

(*b*) The solution of the patching method with an input Bloch wave [Fig. 2(ii)] stabilizes faster as expected.

(*c*) The right part of the solution of a simple top-hat multislice with an input Bloch-wave solution [Fig. 2(iii)] matches the corresponding stable regions of Figs. 2(i), (ii), although if the multislice iterates further, it will be completely deteriorated.

(*d*) The Bloch-wave solution in the first slice of Figs. 2(ii) or (iii) here is close to the final solution.

For completeness, it should be mentioned that the Bloch-wave solutions were terminated exactly halfway between the atoms.

A more complicated example is shown in Figs. 3(i), (ii), an artificial 2×1 reconstruction of the Au(001) surface. In this case one can see the expected changes in the Bloch-wave solution due to the different surface-termination structure. Fig. 3(ii) shows the RHEED patterns corresponding to Fig. 3(i). They are Fourier transforms of the vacuum waves excluding the patched area in the slices in Fig. 3(i). The reconstruction spots occur in those stabilized patterns.

The final most interesting and probably most controversial result is for the Au(110) surface in the [1$\bar{1}$0] zone and is shown in Fig. 4. What is clear from this result is that the initial Bloch-wave solution is not a good guess of the true solution. As shown by a comparison between the two RHEED patterns, owing to the initial Bloch-wave solution and final patched solution in Fig. 5, the Bloch-wave form does not contain any of the bulk forbidden spots but the final form does and the Bloch-wave form contains the surface forbidden spots but the final form does not. We will discuss this in more detail below.

IV. Discussion

The Bloch-wave approach that we proposed in previous papers (Ma & Marks, 1989, 1990*a*, *b*) appears to be working very well for the Au(001) surface in the [010] zone (Fig. 2), but it seems wrong for the Au(110) surface in the [1$\bar{1}$0] zone (Fig. 4).

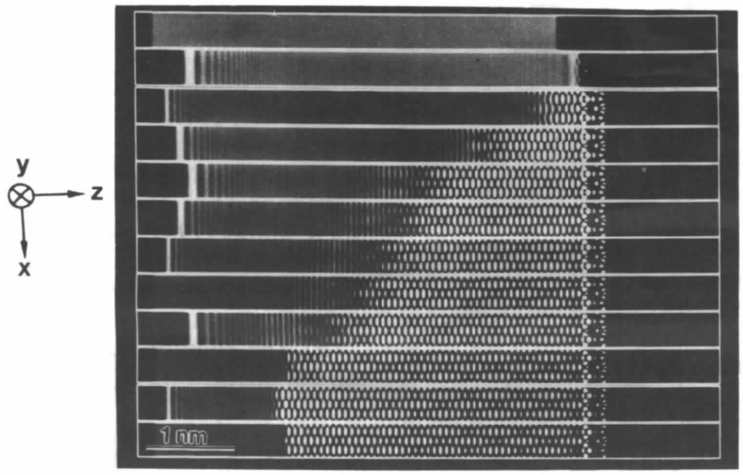

(i)

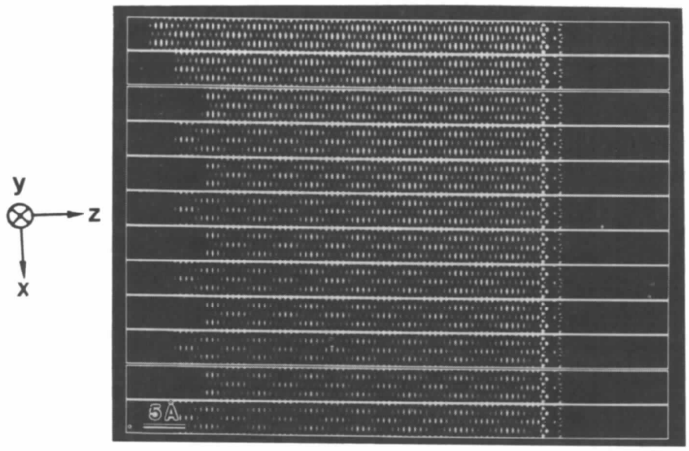

(ii)

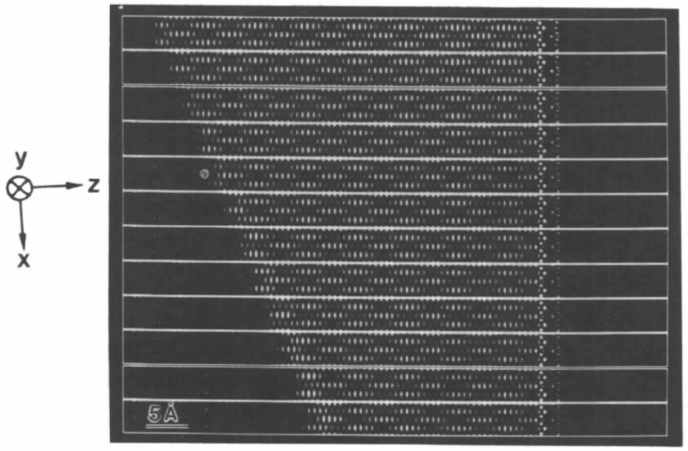

(iii)

Fig. 2. (i) Wave fields calculated using the edge-patching method with an incident plane wave. (ii) Wave fields calculated using the edge-patching method with an input Bloch-wave solution. (iii) Wave fields calculated by a simple top-hat multislice with an input Bloch-wave solution. All these calculations are for the Au(001) surface in the [010] zone. The incident angle is 30 mrad and absorption 10%. The incident electron energy is 100 keV. The series of slice numbers for (i)–(iii) is: 1, 100, 300, 600, 900, 1000, 1100, 1200, 1300, 1500, 1700, 2050. The thickness of each iteration Δy is 1·012 Å.

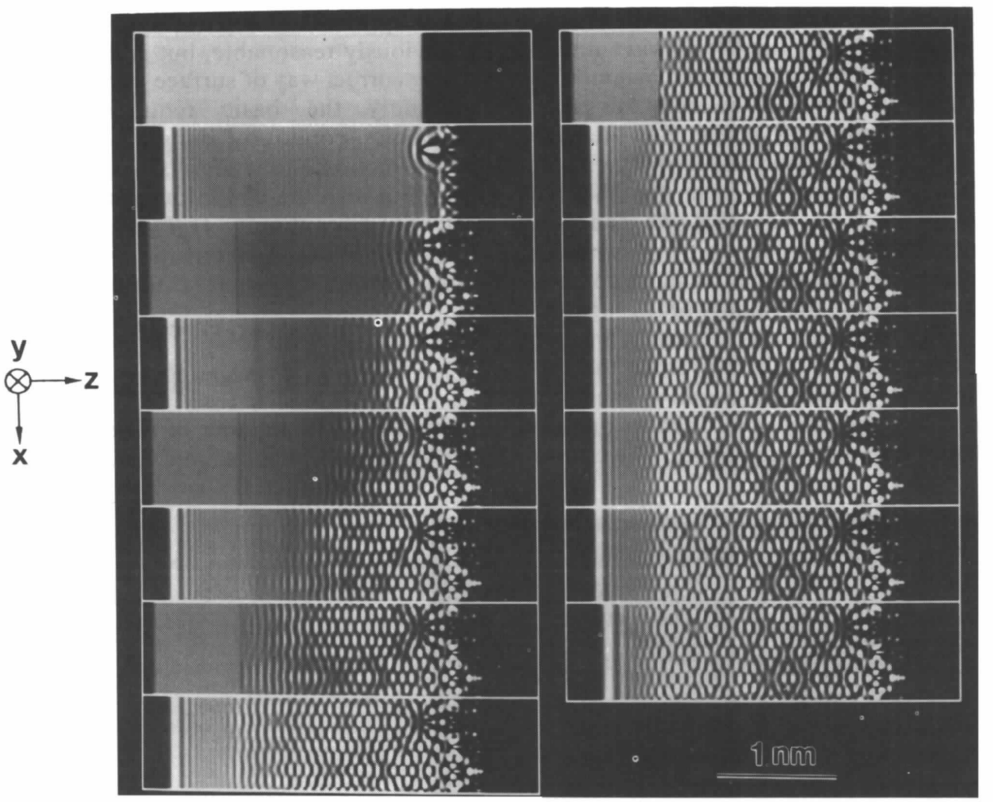

(i)

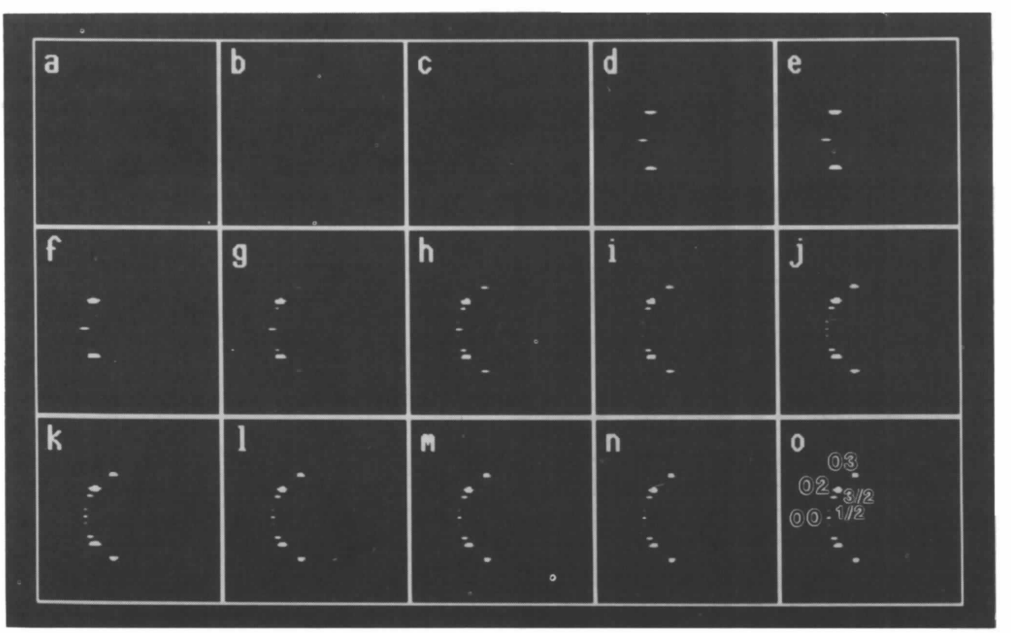

(ii)

Fig. 3. (i) Wave fields calculated for the 2×1 Au(001) surface in the [010] zone using the edge-patching method. The series of output slice numbers is: 1, 100, 200, 300, 400, 500, 600, 700, 800, 900, 1100, 1300, 1500, 1700, 2050. The rest of the conditions are the same as for Fig. 2. (ii) RHEED patterns corresponding to (i). They are Fourier transforms of the vacuum wave excluding the patched areas, which are shown in the range from *B* to *C* in Fig. 1.

First, let us consider the symmetry of the electron wave function generated by the Bloch-wave method with matching on a plane, which is the symmetry of the primitive unit cell. However, owing to the surface termination the real physical system has the lower symmetry of the complete unit cell. The Bloch-wave solution within the crystal is exact for the bulk material and there is no way that we can force eigensolutions with the complete unit-cell symmetry, even if you reduce the matrix from the more complete form that we have used to the smaller set as suggested by Kambe (1988); the solutions can only have the symmetry of the primitive unit cell. Since the form of the wave solution outside the crystal is exact, that inside is also exact, the only area open to question is the matching of the two at the surface. The conventional approach of a plane surface for the matching is obviously reasonable, but is it correct?

The correct way of surface matching should satisfy not only the basic requirement of quantum mechanics, continuity along a boundary of both the wave function and its derivative normal to the boundary, but also the condition of a minimum artificial potential discontinuity. If $\Psi(\mathbf{r})$ is the wave inside the crystal, $\Phi(\mathbf{r})$ the wave outside, then for the matching surface $\mathbf{s}$ with a normal vector $\mathbf{n}$ we have

$$\Phi(\mathbf{r}) = \Psi(\mathbf{r})|_{\mathbf{r}=\mathbf{s}} \tag{5}$$

$$\mathbf{n} \cdot \nabla[\Phi(\mathbf{r}) - \Psi(\mathbf{r})]|_{\mathbf{r}=\mathbf{s}} = 0. \tag{6}$$

There are a vast number of different surfaces which can be chosen as matching surfaces on which these

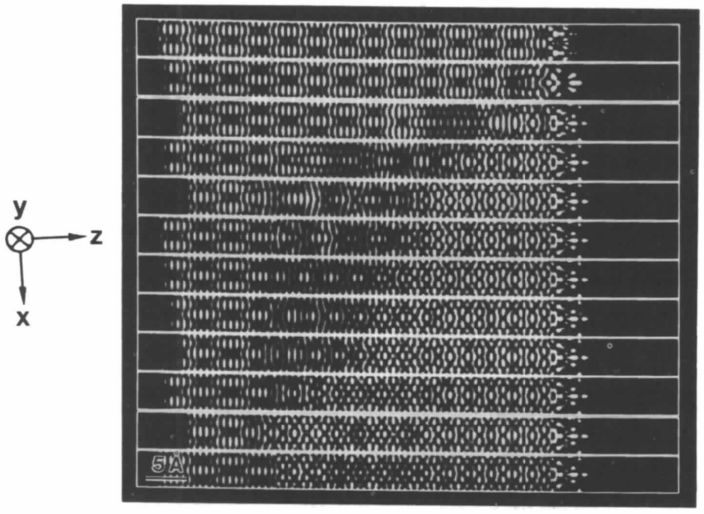

Fig. 4. Wave fields calculated for the Au(110) surface in the [1$\bar{1}$0] zone with a top-hat Bloch-wave input. The rest of the conditions are the same as for Fig. 2. The first slice shows the Bloch-wave solution and the last three slices show stabilized multislice solutions with the edge-patching method.

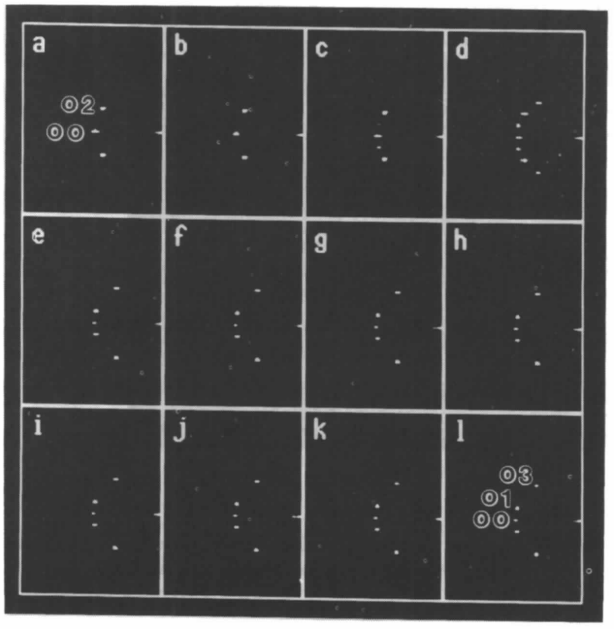

Fig. 5. RHEED patterns corresponding to Fig. 4. The incident spot in each pattern is masked, therefore the first three patterns (*a*)–(*c*) do not show any spot since the reflection is weak at the beginning of the iteration.

boundary conditions are imposed, but the one of interest should be the one with the minimum potential discontinuity. It can be shown that it should satisfy the following condition (Appendix I):

$$\mathbf{n} \cdot \nabla V(\mathbf{r})|_{\mathbf{r}=\mathbf{s}} = 0. \quad (7)$$

For the Au(001) surface in the [010] zone, a plane boundary between the atoms automatically satisfies (7) because it has the maximum potential (close to zero) along the surface normal **n**, see Fig. 6, and the change in the Bloch-wave solution with iteration cycle is the accommodation of this small potential discontinuity. However, for the Au(110) surface in the [1$\bar{1}$0] zone, (7) cannot be satisfied by a simple plane surface and the imposed potential discontinuity will be substantial (Fig. 6). This discontinuity is responsible for the large deviations in Fig. 4. As outlined in Appendix II, it is necessary and also possible to modify the Bloch-wave boundary conditions by taking a non-planar surface for the boundary match.

An important point that should be mentioned is that the boundary-match issue herein may also be relevant to transmission surface imaging in plan view; certainly one can easily see that it will affect Bloch-wave calculations of surface step contrast in plan view where the same issues will arise. This merits further exploration, although we should note that the importance of the effect will fall as the wave vector normal to the surface increases and will therefore presumably be far smaller.

Let us now discuss the patching approach. For completeness, it should be mentioned that the idea of edge patching is simple and the initial ideas of a self-consistent RHEED solution have been discussed earlier (Cowley, Marks & Spence, unpublished; Howie & Marks, unpublished). What is significant from these results is that the edge-patching method for reaching a self-consistent RHEED solution does appear to work very well and can be applied (computer time permitting) to any surfaces. What remains is of course the worrying question of how well it matches experiments and how perfect experimental results are.

This work was supported by the National Science Foundation, grant nos. DMR 85-20280 and DMR 87-17376.

APPENDIX I

We will prove here that (7) in the text corresponds to the best matching surface for the Bloch-wave method. Let $V(\mathbf{r})$ be a truncated Bloch potential and $V'(\mathbf{r})$ be the true potential. The difference between the two is a perturbation potential which will introduce additional scattering which is not included in the Bloch-wave solution. To minimize this perturbation, we want to minimize the first (and higher) perturbation term, which is equivalent to minimizing

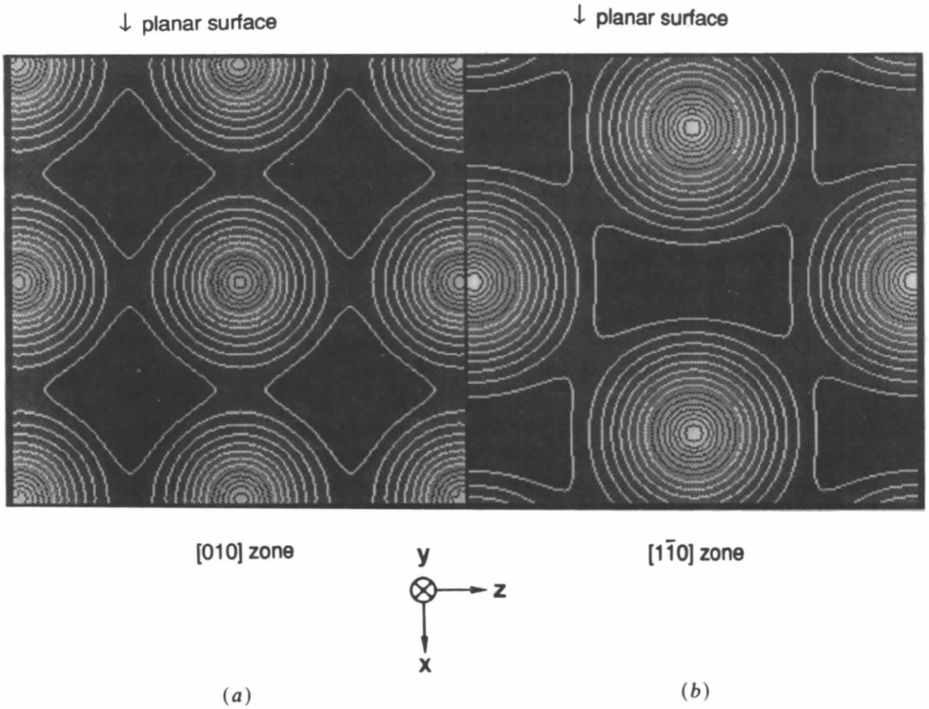

Fig. 6. Diagrams of the projected crystal potential of Au along the [010] (*a*) and [1$\bar{1}$0] (*b*) zones. The white lines are the intersections of equal potential surfaces with the zone plane.

(Born approximation)

$$\int \{V(\mathbf{r}) - V'(\mathbf{r})\} \exp(2\pi i \mathbf{q} \cdot \mathbf{r}) d\mathbf{r} \quad \text{(I-1)}$$

where the integration range is restricted to outside the crystal and $\mathbf{q}$ is the momentum change. With the potentials as sums of atomic potentials (*i.e.* ignoring surface potentials although this does not affect the final result),

$$V(\mathbf{r}) = \sum_{\mathbf{r}_i} v(\mathbf{r} - \mathbf{r}_i) A(\mathbf{r}) \quad \text{(I-2)}$$

where

$$A(\mathbf{r}) = \begin{cases} 1 & \text{for } \mathbf{r} \text{ inside the crystal} \\ 0 & \text{outside} \end{cases} \quad \text{(I-3)}$$

$$V'(\mathbf{r}) = \sum_{\mathbf{r}_i} v(\mathbf{r} - \mathbf{r}_i) B(\mathbf{r}_i) \quad \text{(I-4)}$$

where

$$B(\mathbf{r}_i) = \begin{cases} 1 & \text{for an atom position inside the crystal} \\ 0 & \text{outside.} \end{cases} \quad \text{(I-5)}$$

v here denotes atomic potentials. With the calculus of variation methods, let $A(\mathbf{r})$ go to $A(\mathbf{r}) + \alpha g(\mathbf{r})$ [$g(\mathbf{r})$ defined similarly to $A(\mathbf{r})$] and take the derivative with respect to α for the best surface, *i.e.*

$$\lim_{\alpha \to 0} \partial / \partial \alpha \int \sum_{\mathbf{r}_i} v(\mathbf{r} - \mathbf{r}_i) \{[A(\mathbf{r}) + \alpha g(\mathbf{r})] - B(\mathbf{r}_i)\} = 0 \quad \text{(I-6)}$$

$$\int \delta(\mathbf{r} - \mathbf{s}) g(\mathbf{r}) \mathbf{n} \cdot \nabla \sum_{\mathbf{r}_i} v(\mathbf{r} - \mathbf{r}_i) d\mathbf{r} = 0 \quad \text{(I-7)}$$

where $\mathbf{n}$ is the vector normal to $A(\mathbf{r})$ and $\mathbf{s}$ defines the surface, as used in the main text. Since this must be true for all $g(\mathbf{r})$, it follows that

$$\mathbf{n} \cdot \nabla V(\mathbf{s}) = 0. \quad \text{(I-8)}$$

If there is no external surface potential outside the crystal, then the additional condition $V(\mathbf{s}) = 0$ makes the perturbations vanish to all orders and the Bloch-wave solution is therefore exact.

APPENDIX II

The planar-surface matching can actually be replaced by a periodic non-planar-surface matching, which is numerically feasible. Here, we give an analytical derivation. For the planar-surface matching, $\mathbf{s}$ has the form $z = 0$ and then we have

$$\Phi(\tau, z) = \Psi(\tau, z) \quad \text{(II-1)}$$

$$\partial \Phi(\tau, z)/\partial z = \partial \Psi(\tau, z)/\partial z|_{\tau=(x,y),\, z=0} \quad \text{(II-2)}$$

where Φ is the wave function outside a crystal, Ψ the wave function inside, the surface is set in the xy plane and the surface normal is parallel to the z axis. For a periodic non-planar-surface matching, $\mathbf{s}$ has the form $z = f(x, y)$ and then we have

$$\Phi(\tau, z) = \Psi(\tau, z) \quad \text{(II-3)}$$

$$\partial \Phi(\tau, z)/\partial z = \partial \Psi(\tau, z)/\partial z|_{\tau=(x,y),\, z=f(x,y)} \quad \text{(II-4)}$$

where $f(x, y)$ is a 2D periodic function and its approximate form can be easily derived. Both (II-3) and (II-4) can be expanded as Fourier series:

$$\sum_{\mathbf{g}'} (\delta_{\mathbf{g}'\mathbf{0}'} + R_{\mathbf{g}'}) \exp[i2\pi(\mathbf{k}_{0t'} + \mathbf{g}'_t) \cdot \boldsymbol{\tau}] \times \exp[i2\pi(k_{0z'} + \mathbf{g}'_z) f(x, y)] = \sum_j \varepsilon^{(j)} \sum_{\mathbf{g}} C_{\mathbf{g}}^{(j)} \exp[i2\pi(\mathbf{k}_{0t} + \mathbf{g}_t) \cdot \boldsymbol{\tau}] \times \exp[i2\pi(k_{0z}^{(j)} + g_z) f(x, y)] \quad \text{(II-5)}$$

$$\sum_{\mathbf{g}'} (k_{0z'} + g_{z'})(\delta_{\mathbf{g}'\mathbf{0}'} + R_{\mathbf{g}'}) \exp[i2\pi(\mathbf{k}_{0t'} + \mathbf{g}'_t) \cdot \boldsymbol{\tau}] \times \exp[i2\pi(k_{0z} + g'_z) f(x, y)] = \sum_j \varepsilon^{(j)} \sum_{\mathbf{g}} (k_z^{(j)} + g_z) C_{\mathbf{g}}^{(j)} \exp[i2\pi(\mathbf{k}_{0t} + \mathbf{g}_t) \cdot \boldsymbol{\tau}] \times \exp[i2\pi(k_{0z}^{(j)} + g_z) f(x, y)] \quad \text{(II-6)}$$

where $C_{\mathbf{g}}^{(j)}$ is the coefficient of a plane-wave component $\mathbf{g}$ of a Bloch wave j, $\varepsilon^{(j)}$ excitation coefficients of the Bloch wave j, $R_{\mathbf{g}'}$ the coefficient of a Bragg-reflected wave $\mathbf{g}'$ and δ is Kronecker's delta function.

The exponential terms with $f(x, y)$ in (II-5) and (II-6) can be further expanded as Fourier series, since $f(x, y)$ is a 2D periodic function:

$$\exp[i2\pi(k_{0z'} + g'_z) f(x, y)] = \sum_{\mathbf{h}'} \alpha_{\mathbf{g}',\mathbf{h}'} \exp[i2\pi(\mathbf{k}_{0t'} + \mathbf{h}'_t) \cdot \boldsymbol{\tau}] \quad \text{(II-7)}$$

$$\exp[i2\pi(k_{0z}^{(j)} + g_z) f(x, y)] = \sum_{\mathbf{h}} \beta_{\mathbf{g},\mathbf{h}}^{(j)} \exp[i2\pi(\mathbf{k}_{0t} + \mathbf{h}_t) \cdot \boldsymbol{\tau}] \quad \text{(II-8)}$$

where $\alpha_{\mathbf{g}',\mathbf{h}'}$ and $\beta_{\mathbf{g},\mathbf{h}}^{(j)}$ can be calculated numerically. Substituting (II-7) and (II-8) into (II-5) and (II-6) and letting $\mathbf{g}' + \mathbf{h}' = \mathbf{l}'$ and $\mathbf{g} + \mathbf{h} = \mathbf{l}$, we obtain

$$\mathbf{k}_{0t'} = \mathbf{k}_{0t} \quad \text{(II-9)}$$

$$\xi_{\mathbf{l}} = \sum_j \varepsilon^{(j)} A_{\mathbf{l}}^{(j)} \quad \text{(II-10)}$$

$$k_{0z'} \xi_{\mathbf{l}} = \sum_j \varepsilon^{(j)} B_{\mathbf{l}}^{(j)} \quad \text{(II-11)}$$

where

$$\xi_{\mathbf{l}} = \sum_{\mathbf{g}'} (\delta_{\mathbf{g}'\mathbf{0}'} + R_{\mathbf{g}'}) \alpha_{\mathbf{g}',\mathbf{l}-\mathbf{g}'} \quad \text{(II-12)}$$

$$k_{0z'} \xi_{\mathbf{l}} \cong \sum_{\mathbf{g}'} (k_{0z'} + g'_z)(\delta_{\mathbf{g}'\mathbf{0}'} + R_{\mathbf{g}'}) \alpha_{\mathbf{g}',\mathbf{l}-\mathbf{g}'} \quad \text{(II-13)}$$

$$A_{\mathbf{l}}^{(j)} = \sum_{\mathbf{g}} C_{\mathbf{g}}^{(j)} \beta_{\mathbf{g},\mathbf{l}-\mathbf{g}}^{(j)} \quad \text{(II-14)}$$

$$B_{\mathbf{l}}^{(j)} = \sum_{\mathbf{g}} (k_z^{(j)} + g_z) C_{\mathbf{g}}^{(j)} \beta_{\mathbf{g},\mathbf{l}-\mathbf{g}}^{(j)}, \quad \text{(II-15)}$$

$\varepsilon^{(j)}$ and ξ_l can be solved by (II-10) and (II-11) and then $R_{g'}$ can be solved by (II-12). Although the process as shown here is harder than that for the planar-surface matching, the 2D periodic non-planar-surface matching in principle can be done. In other words, the Bloch-wave method can also be applied to all kinds of periodic planar- or non-planar-surface models.

References

COLELLA, R. (1972). *Acta Cryst.* **A28**, 11-15.
COWLEY, J. M. & MOODIE, A. F. (1957). *Acta Cryst.* **10**, 609-619.
COWLEY, J. M. & MOODIE, A. F. (1959). *Acta Cryst.* **12**, 353-359.
ISHIZUKA, K. & UYEDA, N. (1977). *Acta Cryst.* **A33**, 740-749.
KAMBE, K. (1988). *Acta Cryst.* **A44**, 885-890.
MA, Y. (1990*a*). *Proc. XII Int. Congr. for Electron Microscopy, Seattle*, Vol. 2, pp. 372-373. San Francisco Press.
MA, Y. (1990*b*). *Proc. XII Int. Congr. for Electron Microscopy, Seattle*, Vol. 2, pp. 374-375. San Francisco Press.
MA, Y. & MARKS, L. D. (1989). *Acta Cryst.* **A45**, 174-182.
MA, Y. & MARKS, L. D. (1990*a*). *Acta Cryst.* **A46**, 11-32.
MA, Y. & MARKS, L. D. (1990*b*). *Acta Cryst.* **A46**, 594-606.
MA, Y. & MARKS, L. D. (1991). Submitted to *J. Electron. Microsc. Tech.*
MAKSYM, P. A. & BEEBY, J. L. (1981). *Surf. Sci.* **110**, 423-436.
MARKS, L. D. & MA, Y. (1988). *Acta Cryst.* **A44**, 392-393.
METHERELL, A. J. (1975). *Electron Microscopy in Materials Science*, edited by U. VALDRE & E. RUEDL, Vol. 2, pp. 401-550. Luxembourg: Commission of the European Communities.
MOON, A. R. (1972). *Z. Naturforsch. Teil A*, **27**, 390-401.
PENG, L. M. & COWLEY, J. M. (1986). *Acta Cryst.* **A42**, 545-552.
SHINOHARA, K. (1932). *Inst. Phys. Chem. Res. (Tokyo)*, **18**, 223-236.

Acta Cryst. (1991). A47, 715-723

Structure Retrieval in HREM

BY M. A. GRIBELYUK*

Institute of Crystallography, USSR Academy of Sciences, Leninskii Prospekt 59, 117333 *Moscow, USSR*

(*Received* 25 *June* 1990; *accepted* 17 *May* 1991)

Abstract

A new iteration method for direct structure retrieval starting from the exit plane-wave function $\Psi_e(\mathbf{r})$ is proposed and tested on models. The imaginary part of the potential cannot be retrieved. The effects of the limited resolution of $\Psi_e(\mathbf{r})$ as well as neglect of high-order Laue-zone effects and the choice of the starting potential on the result are discussed. The procedure is found to be preferable to that based on the subsequent approximation method with respect to a higher convergence rate. It is shown that an error as low as 10% may be obtained for the real part of the retrieved potential up to $|\sigma V(\mathbf{r})t| < 5$.

1. Introduction

As is well known, the image-formation process in high-resolution electron microscopy (HREM) is influenced by dynamical scattering effects and distortions caused by the electron-optical system of the microscope. Therefore the image interpretation is mostly based on results of computer simulation. If the initial structure motif is known (from X-ray analysis data, for example) or a structure is postulated, the matching procedure allows one to refine both the structural details and the experimental conditions under which the image has been obtained and to interpret the images of structure defects as well.

We should point out some disadvantages of this approach. Firstly, the trial-and-error nature of the simulation process leads to considerable expense of computer time and depends on the experience of the researcher. Secondly, it cannot be applied to the investigation of unknown structures.

The elaboration of direct structure-restoration methods seems to be attractive in this respect. The problem may be treated as consisting of two parts:

(*a*) correction for the transfer function of the microscope, *i.e.* restoration of the wave function at the exit plane of a crystal from the EM image(s);

(*b*) inversion of the dynamical diffraction, *i.e.* restoration of the lattice potential $V_e(r)$ from the exit plane wave function.

The dynamical scattering effects and the influence of the electron-optical system are therefore considered separately and this makes it possible to find independently the most efficient method for the solution of each problem.

Approaches aimed at restoration from the exit plane wave function include defocus series processing and transmission electron microscopy/scanning transmission electron microscopy (TEM/STEM) electron holography. Non-linear image processing methods have been suggested by Kirkland (1982,

* Now on leave: Department of Physics, Arizona State University, Tempe, AZ 85287-1504, USA.

0108-7673/91/060715-09$03.00 © 1991 International Union of Crystallography